DOI: 10.13009/EUCASS2019-362

Numerical Solution of Supersonic Gas-Solid Two-Phase Flow

Xiang Zhao[a,b], Zhixun Xia[a], Likun Ma[a], Dan Michaels[b], Benveniste Natan[b], Chaolong Li[a]

[a] Department of Aerospace Science and Engineering, National University of Defense Technology, Changsha, Hunan, 410073, P. R. China

[b] Faculty of Aerospace Engineering, Technion - Israel Institute of Technology, Haifa, 32000, Israel

Abstract

A solver, namely rhoGasSolidFoam, has been developed on the OpenFOAM platform to solve a supersonic gas-solid two-phase flow. The Reynolds-averaged Navier-Stokes equations have been employed and solved using a density-based compressible code based on OpenFOAM with the Euler scheme. The Reynolds stress has been solved using a standard k-ε model. An optimized chemical mechanism has been employed for CH_4/CO/H_2 syngas reaction. The PaSR model has been adopted to solve RANS governing equations for reactive flows. The solid particles have been solved by the Lagrangian method. Radiation, as well as mass and heat transfer between solid particles and gas, and the surface combustion of solid particles have been taken into consideration. A 3-step global chemical mechanism has been adopted for carbon surface combustion. Validations using experimental data of DLR and ramjet combustors show that numerical results agree well with experimental results, indicating that the rhoGasSolidFoam can be used to calculate both supersonic gas reactive flows and gas-solid two-phase reactive flow. Thus, it can be inferred that the rhoGasSolidFoam is applicable to solving supersonic gas-solid two-phase reactive flows as well as solid-fuel scramjets. The numerical results of the solid-fuel scramjet show that it can operate well. However, the combustion efficiency of solid particles is pretty low, which certainly affects the performance.

1. Introduction

Recently, an increased interest on Solid-Fuel Scramjets has been observed. The solid-fuel scramjet is an interesting option for a supersonic combustion ramjet because of significant advantages such as simple fuel supply systems and compactness, however, adjustable thrust and re-ignition are difficult to achieve [1, 2].

Solid-Fuel Scramjets can be classified into two types. One is the supersonic combustor with solid-fuel grains connected to the wall, as shown in Fig. 1. Solid-fuel grains react with oxygen after decomposition and gasification. The cavity is employed to obtain self-ignition and flame stabilization. The interior configuration changes a lot during combustion, resulting in the deterioration of capability to stabilize the flame. The other type is the scramjet with solid propellant based gas generator, shown in Fig. 2. The solid propellant itself has a limited amount of oxidizer, which contributes to the combustion of solid propellant inside the gas generator. Fuel-rich hot gas containing solid particles is injected into the supersonic combustor for further reaction. The high temperature of the gas benefits ignition and flame stabilization. The air to fuel ratio is adjustable and the combustor can operate stably as long as the solid propellant is not consumed up.

DOI: 10.13009/EUCASS2019-362

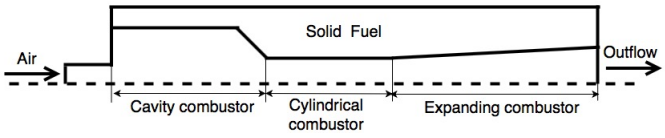

Fig. 1 Schematic of one type of solid-fuel scramjet

Institutes like the US Naval Postgraduate School [3, 4], Technion - Israel Institute of Technology [5-10], University of Rome [11], Beijing Institute of Technology [12-17], Northwest Polytechnical University [18] and National University of Defense Technology [1, 2, 19] have carried out investigations on solid-fuel scramjets. Most numerical simulations were conducted with FLUENT where the kinetic model employed one or several steps global reactions and the combustion model was based on eddy-dissipation. Ben-Arosh [6, 7] employed simplified 2-equation ethylene combustion model for theoretical study of a solid fuel scramjet combustor. The chemical reactions as well as the species production rates were calculated by the CHEMKIN chemical kinetics package combined with the PHOENICS code. Simone [11] adopted a six-species three-step simplified mechanism to simulate gas-phase combustion of solid-fuel scramjet engines fueled with Lithium Hydride (LiH). The coupling between chemical kinetics and turbulence was modeled using the eddy dissipation concept model. Xinyan Pei [12, 13] used a global one-step reaction for the combustion process of C_4H_6 and the non-premixed equilibrium PDF (probability density function) approach for the turbulent combustion model to simulate a solid-fuel scramjet combustor fueled with hydroxyl-terminated-polybutadiene (HTPB). Wang, Chi and Hu [15-17] employed a global one-step irreversible reaction mechanism for the combustion model of $C_5H_8O_2$, as well as the finite rate/eddy dissipation model for the chemistry-turbulent interaction to study a solid-fuel scramjet combustor fueled with PMMA. Liu [18] adopted a four, single-step overall reaction mechanisms that includes surface reaction of carbon and boron particles. The eddy-dissipation model was used as the gas phase combustion model, and the diffusion-limited model was used as the heterogeneous phase surface reaction model. Zhao [2] employed two one-step global reaction mechanisms for the combustion as well as the eddy-dissipation model for the chemistry-turbulent interaction.

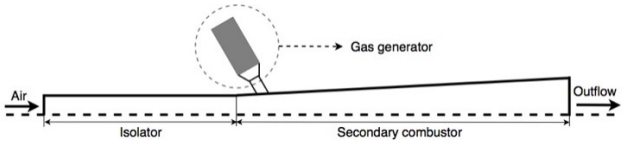

Fig. 2 Schematic of the other type of solid-fuel scramjet

Simplified global reaction mechanisms where intermediate products are not taken into consideration could lead to overestimated temperature. Moreover, solid particles have not been considered in most calculations. Although Liu [18] considered both carbon and boron particles, the surface reaction was merely single step for each kind of particle. The gas-solid interaction employed diffusion-limited model, which neglected the kinetics. These models are so simplified that may result in large deviations from the reality and in differences between various studies [20-23]. Accurate models and precise calculations are fundamental to study movements and combustion of solid particles as well as solid-fuel scramjets. In addition, as we all know, the commercial software is a black box, which means that details of each sub-model are hidden for us. Thus, the expansibility is limited. Moreover, using ANSYS FLUENT costs a lot due to the high price. Therefore, it is necessary to develop a set of numerical codes with high fidelity and flexibility based on the open-source software packages [24].

The present paper exhibits the results of the solver, namely rhoGasSolidFoam, which is developed on

the OpenFOAM platform. Since there are no experimental results concerning supersonic gas-solid two phase reactive flows in open literature, validations of the solver and related models employ the data of DLR experiments and ramjet experiments. A case of solid-fuel scramjet with a solid propellant based gas generator has been analyzed and presented.

2. Models and Methods

2.1 Gas phase modeling

In rhoGasSolidFoam the influence of the solid volume fraction is not included. The gas phase is compressible fluid.

The continuity conservation equation:

$$\frac{\partial(\rho_g)}{\partial t} + \nabla \cdot (\rho_g u_g) = S_m$$

Here, u_g and ρ_g denote the velocity and density of gas phase, respectively. S_m is the source term.

The momentum conservation equation:

$$\frac{\partial}{\partial t}(\rho_g u_g) + \nabla \cdot (\rho_g u_g u_g) - \nabla \cdot (\tau_g) - \nabla \cdot (\rho_g R_g) = -\nabla p + \rho_g g + S_u$$

Where p and τ_g are pressure and shear stress. g and R_g are the gravitational acceleration and Reynold stress tensor, respectively. S_u is the source term.

The energy conservation equation:

$$\frac{\partial(\rho_g h)}{\partial t} + \frac{\partial(\rho_g K)}{\partial t} + \nabla \cdot (\rho_g u_g h) + \nabla \cdot (\rho_g u_g K) - \nabla \cdot (\alpha_{eff} \nabla(h)) = \nabla p + \rho_g u_g g + S_h$$

Here, h, K, α_{eff} are the enthalpy, kinetic energy and effective turbulent thermal diffusivity. S_h is the source term.

Species transport equation:

$$\frac{\partial \rho_g Y_i}{\partial t} + \nabla \cdot (\rho_g u_g Y_i) - \nabla \cdot (D_{eff} \nabla(\rho_g Y_i)) = S_i$$

Where Y_i is the mass fraction of the species, while D_{eff} is the mass diffusivity. S_i is the source term.

2.2 Particle phase modeling

Solid particles are assumed spherical. According to Faeth's work [25], Basset and virtual mass forces are neglected due to the high density ratios studied here. Particle motion is governed by Newton Second Law. The resulting relation for particle drag force and drag coefficient are given as follows:

$$F_p = C_D \frac{1}{8} \pi d_p^2 \rho |u_p - u_g| (u_p - u_g) - \frac{\pi}{6} d_p^3 \nabla p + \frac{\pi}{6} d_p^3 \rho_p g$$

$$C_D = \begin{cases} 0.424, & if\ Re_p \geq 1000 \\ \frac{24}{Re_p}(1 + \frac{1}{6} Re_p^{2/3}, & otherwise \end{cases}$$

$$Re_p = \frac{\rho_g |u_p - u_g| d_p}{\mu}$$

where F_p is the drag force, while Re_p is the particle Reynolds number.

DOI: 10.13009/EUCASS2019-362

2.3 Source terms

The source terms are calculated by summing the force, energy and mass transfer contributions from each individual particle in the computational cell. Dividing this summation by the cell volume gives the following relations for particle momentum, enthalpy and specie mass transfer source terms[26]:

$$S_m = \sum_{k=1}^{N_k} S_i$$

$$S_u = -\frac{1}{V}\sum_{V} N_p F_p$$

$$S_h = \left[-\frac{1}{V}\sum_{V} N_p\left(H_p + Q_{s,p} + Q_{r,p}\right)\right] + \sum_{r=1}^{N_g} q_r \omega_r$$

$$S_i = \left[-\frac{1}{V}\sum_{V} N_p m_{p,i}\right] + \sum_{r=1}^{N_g} \omega_r$$

here, N_p is the number of physical particles represented by a single Lagrange group. $m_{p,i}$ is the summation of specie mass transfer from the particle due to surface reactions. H_p is the rate of heat transfer between the particle and gas. $Q_{s,p}$ is the rate of energy release from the surface reactions. $Q_{r,p}$ is the radiation between gas and solid phases. q_r is the heat release from the gas reaction. ω_r is the generation rate of gas.

2.4 Chemical reaction models

For the gas-solid two-phase supersonic flow, the chemical reaction processes include heterogeneous and homogeneous reactions.

2.4.1 Particle surface reactions

Table 1 Products of fuel-rich solid propellant

Phase	Specie	Mass fraction
Gas (51.2%)	CH_4	7.2%
	H_2	19.6%
	CO	59.3%
	N_2	13.9%
Solid (48.8%)	C	100.0%

In the current work, a HTPB/AP solid propellant is assumed as fuel for a solid-fuel scramjet. According to the calculation results by CEA, products are listed in Table 1 under the condition of ignoring species that account few mass fractions. The heterogeneous combustion is specified based on a three-step carbon surface reaction mechanism [27].

$$C(s) + 0.5O_2 \rightarrow CO$$

$$C(s) + CO_2 \rightarrow 2CO$$

$$C(s) + H_2O \rightarrow CO + H_2$$

The mass of carbon particles reduces due to the surface reactions. Oxygen, carbon dioxide and water vaper in the vicinity are consumed, and carbon monoxide as well as hydrogen is produced. The products are added into the flow for further combustion. The rate of surface reaction is specified assuming a

DOI: 10.13009/EUCASS2019-362

kinetic-diffusion limited process [20].

$$\frac{\partial m_s}{\partial t} = A_k \left[\frac{1}{C_d} + \frac{1}{C_{ch}}\right]^{-1} \rho RT \frac{Y_s}{M_s}$$

$$C_d = C \frac{[(T + T_k)/2]^{0.75}}{d_k}$$

$$C_{ch} = Aexp(-\frac{E_a}{RT_k})$$

C_d and C_{ch} denote the surface kinetic rate and diffusion mass transfer rate, respectively. The kinetic parameters of the three-step surface reaction are listed in Table 2 [21, 27]. The diffusion rate is assumed 5×10^{-12} kg/m·s·Pa·$K^{0.75}$ [21, 28]. A shrinking core model has been employed to denote particle diameter variation for heterogeneous reactions.

Table 2 Kinetic parameters for heterogeneous reactions

	Reactions	A (kg/m²·s·Pa)	E_a (kg/mol·K)
R1	$C + 0.5O_2 \rightarrow CO$	0.016	65.9
R2	$C + CO_2 \rightarrow 2CO$	6.35×10^{-3}	162
R3	$C + H_2O \rightarrow H_2 + CO$	1.92×10^{-3}	147

2.4.2 Gas reactions

From Table 1, combustible gases are $CH_4/H_2/CO$, which will react with inlet air in the supersonic combustor. As a matter of fact, there are hundreds of gas reactions occurring during syngas combustion. For saving computational resources and speeding up calculations, a simplified syngas skeletal mechanism has been employed based on Ref. [29]. Moreover, a comprehensive H_2/O_2 kinetic model [30] has been employed to validate the calculations with DLR experiments. Turbulence-combustion/gasification interaction has been modeled by partially stirred reactor (PaSR) model.

3. Computational details

3.1 Numerical scheme

There are some standard solvers for simulating gas-solid flow in the open-source software package, OpenFOAM v1806 [31]. Specifically, rhoReactingFoam is a solver that can model supersonic gas reactive flow, while coalChemistryFoam is suitable for dilute reactive gas-solid two-phase flow. In order to simulate supersonic gas-solid two-phase flow, we have developed a new solver based on the advantages of these two standard solvers. The solver completes its functions (*e.g.*, particle motion, heat and mass transfer, and chemical reactions) via calling various libraries. A three-step kinetic-diffusion limited char surface reaction library is implemented for heterogeneous reactions. Both the combustible gases and combustion enthalpy produced by char surface reaction are added into the reactive gas flow.

The governing equations of gas phase are discretized by finite volume method. The variables are stored on collocated grids. Central Differencing Scheme is used for the convective terms and diffusion terms. Euler scheme is employed for time integration. The cell-vertex method is chosen for interpolation between Eulerian and Lagrangian spaces. The PIMPLE algorithm is adopted for handling pressure and velocity.

Due to the limitations in computing resources, the Reynolds-averaged Navier-Stokes equations have

been employed in the simulations. The Reynolds stress has been solved using a standard k-ε model. A 17-species 49-step skeleton mechanism for syngas combustion and a 13-species 27-step mechanism for hydrogen combustion have been employed [29, 30].

3.2 Computational conditions

3.2.1 The case of supersonic gas reactive flow

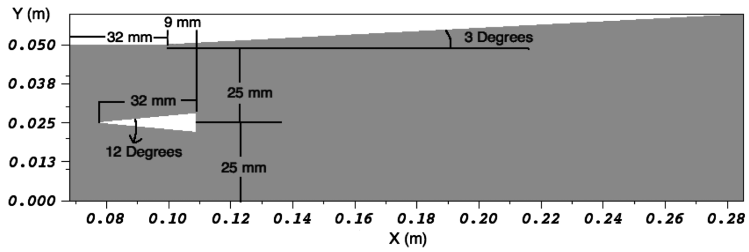

Fig. 3 Combustor model configuration and inflow conditions [34]

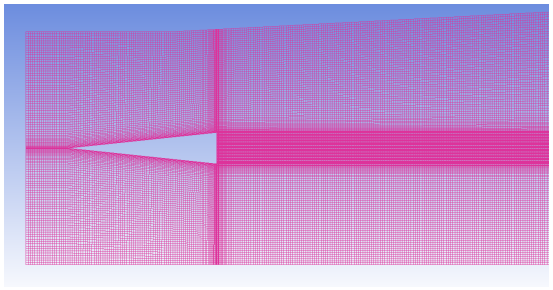

Fig. 4 Schematic of the computational mesh for gas reactive flow

Table 3 Inflow conditions for gas reactive flow [34]

Property	Freestream	Injector holes
U_∞, m/s	730.0	1200.0
T_∞, K	340.0	250.0
P_∞, bar	1.0	1.0
Y_{N2}	0.736	0.0
Y_{O2}	0.232	0.0
Y_{H2}	0.0	1.0
Y_{H2O}	0.032	0.0

In order to validate the solver for supersonic gas reactive flow, a model scramjet studied at the Institute of Chemical Propulsion of the DLR, German Aerospace Center [32, 33] has been simulated using a RANS method. The combustor configuration is shown in Fig. 3 and inflow conditions are listed in Table 3 [34]. For simplification, a cyclic narrow domain with only one injector has been employed in the simulation. The case consists of 2.1M cells. Schematic of computational mesh is shown in Fig. 4. The grids are both refined at the boundary layer of wedge-wall and the inlet of fuel. Slip boundary conditions on the upper and lower walls of the combustor are assumed according to the article [35].

3.2.2 The case of gas-solid two-phase reactive flow

Ducted rocket experiments conducted by Kim [21] have been simulated to validate the solver for solid-

DOI: 10.13009/EUCASS2019-362

gas two-phase reactive flow. There are 46 groups of experiments in total. We adopted one of the two two-inlet configurations (AI2-180) which accounts 11 of the 46 experiments. The combustor configuration is shown in Fig. 5 and the geometric specifications are listed in Table 4. According to the experimental data, boundary conditions are summarized in Table 5. Components of fuel-rich gas are listed in Table 6. Hexahedral structured grids of a half-domain with 0.6M cells have been adopted during calculations. Non-slip wall is assumed. The volume fraction of gas is more than 99% by calculation. Thus the solver can be used to simulate the case.

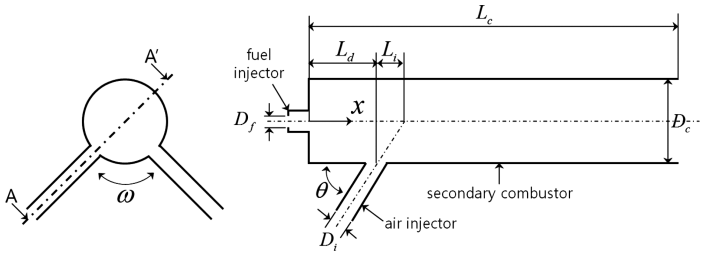

Fig. 5 Schematic of the ducted rocket combustor [21]

Table 4 Geometries of the combustor

Parameters	AI2-180
ω, deg	180
θ, deg	60
D_i, mm	16.5
D_f, mm	4.8
D_c, mm	103
L_c, mm	490
L_d, mm	70
L_i, mm	30

Table 5 Boundary conditions for solid-gas two-phase flow

Property	Air	Fuel-rich gas
U_∞, m/s	The experimental data	556
T_∞, K	535	1164
P_∞, bar	5.3	The experimental data*

The experimental data: specific parameters should accord to the experimental data.

The experimental data: total pressure should be set according to the experimental data.*

Table 6 Components of fuel-rich gas

Phase	Component	Mass fraction	Total
Solid phase	C	0.266	0.266
Gas phase	H_2O	0.0255	0.734
	H_2	0.0708	
	CO	0.2587	
	CO_2	0.0131	
	CH_4	0.0460	
	N_2	0.5859	

DOI: 10.13009/EUCASS2019-362

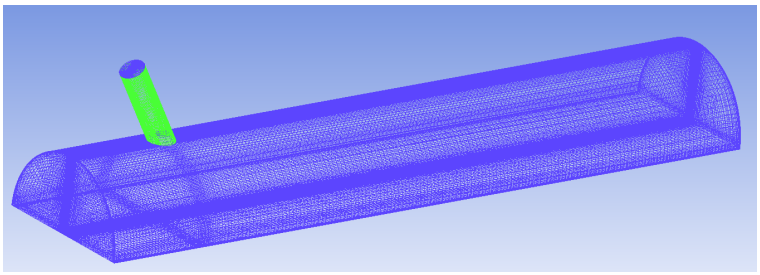

Fig. 6 Schematic of the computational domain for gas-solid two-phase reactive flow

3.2.3 The case of solid-fuel scramjet

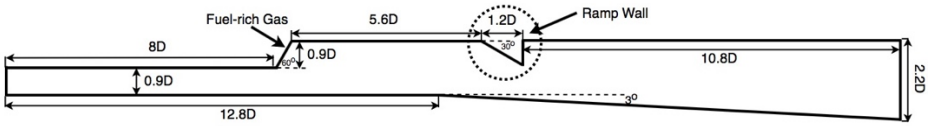

Fig. 7 Schematic of the solid-fuel scramjet

Based on researcher's achievements, we have proposed a certain configuration of solid-fuel scramjet. As shown in Fig. 7, a solid propellant based gas generator is used to provide fuel-rich hot gas and solid particles. A 30° ramp wall is employed to obtain flame ignition and stabilization. D is the width of the combustor. Components of fuel-rich gas are listed in Table 1. Details of boundary conditions are shown in Table 7, which simulates the solid-fuel scramjet operating at the equivalence ratio of 0.5. The volume fraction of gas is more than 99% by calculation, denoting that the solver can be used to simulate the case.

Table 7 Boundary conditions of solid-fuel scramjet

Property	Air	Fuel-rich gas
U_∞, m/s	1350	1044
T_∞, K	739	1288
P_∞, bar	0.87	2.0

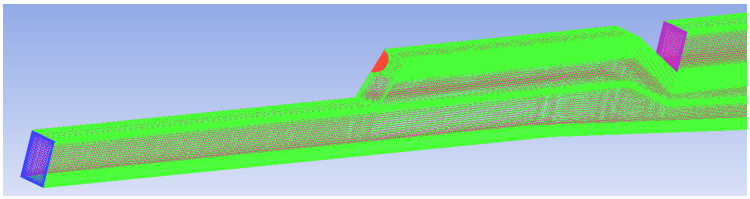

Fig. 8 Schematic of the computational mesh for supersonic gas-solid two-phase reactive flow

4. Results and discussion

4.1 Validations

4.1.1 The case of supersonic gas reactive flow

From Fig. 9, we have compared predicted and experimentally measured axial velocity for the non-reacting case. The overall agreement is good but the velocity in the low-pressure recirculation region is overpredicted. This is related to k-ε turbulent model, which is not very suitable to capture the details of

DOI: 10.13009/EUCASS2019-362

flow parameters where the velocity gradient is extremely high. From Fig. 10 and Fig. 11, reacting cases also show good agreement between calculations and experiments. However, there are some discrepancies, especially in the recirculation region just after the jet exits the wedge. Generally, the deviations are acceptable and the results of the calculation denote that the solver and related models can be used to simulate the supersonic gas reactive flow.

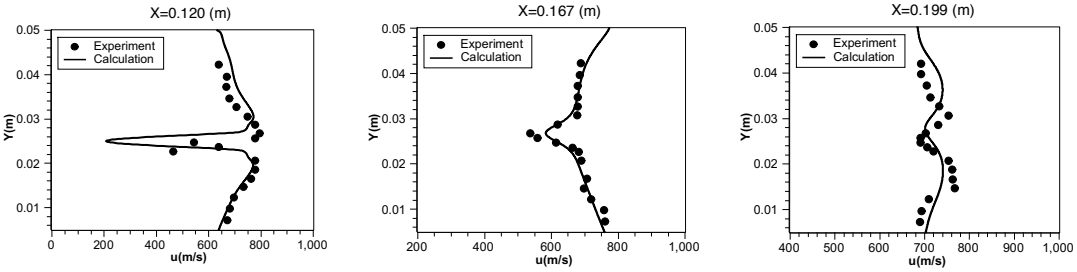

Fig. 9 Axial velocity profiles for the non-reacting case

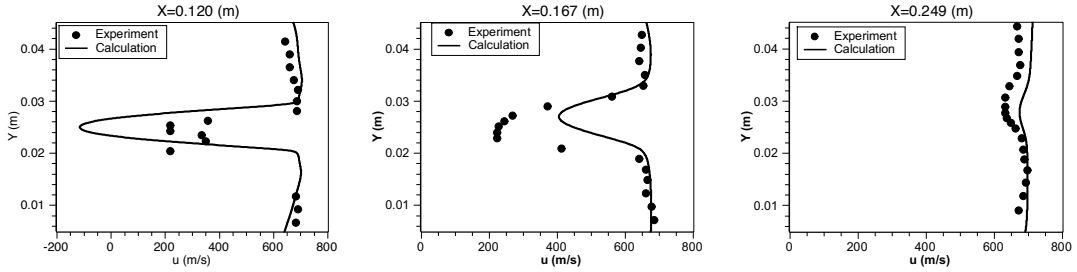

Fig. 10 Axial velocity profiles for the reacting case

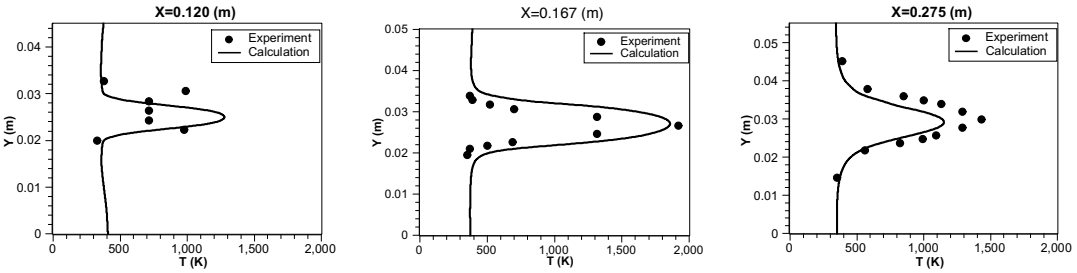

Fig. 11 Static temperature profiles for the reacting case

DOI: 10.13009/EUCASS2019-362

4.1.2 The case of gas-solid two-phase reactive flow

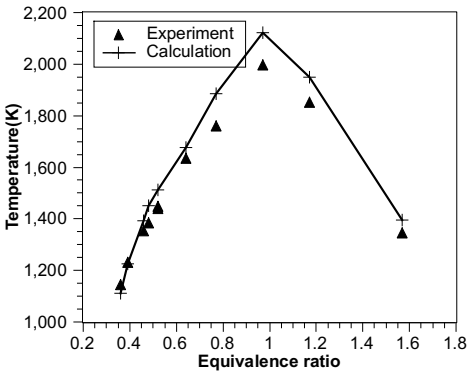

Fig. 12 Static temperature of the combustor at different equivalence ratio

The static temperature versus the equivalence ratio is shown in Fig. 12. The numerical results agree well with the experimental data though there are some deviations. The numerical temperature is slightly higher. This can be attributed to the adiabatic wall in the simulation, where the heat flux between the flow and wall are ignored. The higher the temperature is, the higher is the heat flux from the flow to the wall, resulting in the more difference between the numerical and experimental temperature. In addition, the static temperature is evaluated from the characteristic velocity C^* instead of measured directly, leading to deviations to some extent. As we know, there are a few parameters that can be measured in solid fuel ramjet experiments mainly because of limited measure technique. Therefore, there are no more experimental data for comparison. The good agreement indicates that the solver combined with related models is applicable for calculating the gas-solid two-phase reactive flow.

4.2 Analysis of solid-fuel scramjet

In section 4.1, the validations demonstrate that the solver, rhoGasSolidFoam, with related models can be used to solve both supersonic gas reactive flow and gas-solid two-phase reactive flow. Thus, we can conclude that the solver is applicable for supersonic gas-solid two-phase reactive flow. Based on the inference, we have employed the rhoGasSolidFoam to calculate the solid-fuel scramjet described in section 3.2.3.

4.2.1 Flow field characteristics

From Fig. 13, one can see that there are three vortexes in the flow field. One is formed by the interaction of the backward-step and expansion waves and locates behind the ramp wall. The other two which merge into a larger vortex are formed in the cavity which is composed by the backward step and ramp wall. The pressure contours show that the static pressure in the cavity is nearly constant but decreases intensively then fluctuates after the ramp wall. From the temperature contours, the combustion mainly occurs at the high-speed shears and the rear side of the cavity where intensive mass and momentum exchange occur. Velocity and Mach number contours are shown in Fig. 14. The velocity and Mach number of the inlet air decrease in the cavity, where a significant amount of heat is released, but increase after the ramp wall because of the expansion. These contours demonstrate the feasibility of the solid-fuel scramjet as well as the capability of the ramp wall to obtain the ignition and flame stabilization in the supersonic combustor. Fig. 15 shows parameters of carbon particles, including the diameter, temperature and residence time.

DOI: 10.13009/EUCASS2019-362

Carbon particles produced by the gas generator are injected into the supersonic combustor together with fuel-rich hot gas. The combustion of fuel-rich gas releases heat which contributes to raising the temperature. The heat transfer between the solid and gas phases leads to the rise of particles temperature, benefiting the surface reaction of carbon particles. Due to the high speed of inlet flow, the residence time of particles in the supersonic combustor is merely 1.2 ms, which is so short that carbon particles do not have enough time to complete their burning. Thus, the diameter of particles at the outlet is 29 micrometers. In other words, the diameter of carbon particles reduces by only 1 micrometer compared with the initial diameter of 30 micrometers.

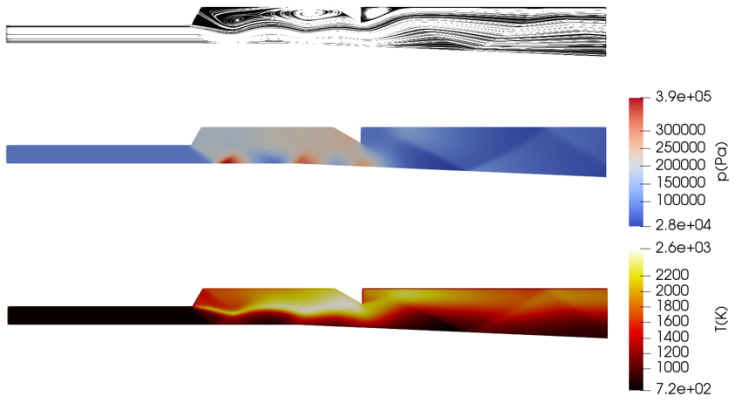

Fig. 13 Streamlines and pressure & temperature contours

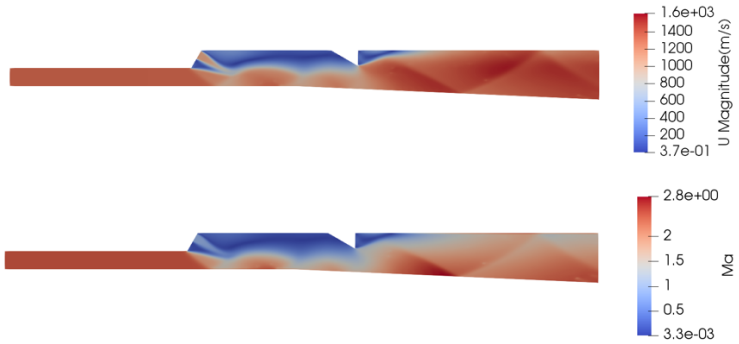

Fig. 14 Velocity and Mach number contours

DOI: 10.13009/EUCASS2019-362

Fig. 15 Parameters of carbon particles

4.2.2 Combustor performance

In order to further demonstrate the feasibility of the solid-fuel scramjet, it is necessary to study the combustor performance, including the combustion efficiency and total pressure recovery.

Due to the differences in the characteristics of combustible gas and carbon particles, the combustion efficiencies are measured separately. The surface combustion of particles produces combustible gases, including CO, CH_4 and H_2. These gases cannot be consumed up in the supersonic combustor, especially for those produced near the outlet. If we take the combustion of these gases into consideration, it is quite complex to assess the combustion efficiency of solid particles. Thus, for simplification, the combustion efficiency of particles is derived based on the mass reduction, which is much easy and convenient for the assessment. It is defined as follow.

$$\eta_{solid} = 1 - \frac{m_{residual,solid}}{m_{initial,solid}}$$

where $m_{residual,solid}$ and $m_{initial,solid}$ are residual and initial mass of solid particles.

The 17-species 49-step skeleton mechanism for syngas combustion results in various intermediate products. Therefore, it is not suitable to assess the combustion efficiency of the gas phase by mass fraction as other researchers did who employed one or several global reactions. The total combustion efficiency of the combustor together with the combustion efficiency of solid phase is employed to evaluate the combustion efficiency of gas phase. The total combustion efficiency is defined as the ratio of the actual rise to the theoretical rise in the total temperature.

$$\eta_{total} = \frac{(m_{air} + m_{fuel})T0_{out,actual} - m_{air}T0_{in}}{(m_{air} + m_{fuel})T0_{out,theoretical} - T0_{in}}$$

here, m_{air} and m_{fuel} represent mass flow rate of inlet air and fuel, respectively. $T0_{out,actual}$ is the actual total temperature obtained by simulation, while $T0_{out,theoretical}$ represents the theoretical total temperature calculated by CEA. $T0_{in}$ is the total temperature of inlet flow.

Then, the combustion efficiency of gas phase can be derived as follow.

$$\eta_{gas} = \frac{m_{fuel}\eta_{total} - m_{initial,solid}\eta_{solid}}{m_{initial,gas}}$$

DOI: 10.13009/EUCASS2019-362

where $m_{initial,gas}$ is the initial mass flow rate of gas phase.

The total pressure recovery is defined as the ratio of the total pressure at the outlet to that at the inlet.

$$\sigma = \frac{\int P0_{out} dA}{\int P0_{in} dA}$$

here, $P0_{out}$ and $P0_{in}$ represent the total pressure at the outlet and inlet, respectively.

Table 8 Combustor performance of the solid-fuel scramjet

Parameter	Value
Total pressure recovery	33.4%
Combustion efficiency of solid phase	9.6%
Combustion efficiency of gas phase	95.3%
Total combustion efficiency	66.6%

From Table 8, the total combustion efficiency is 66.6% mainly because of the low combustion efficiency of solid phase. The combustion efficiency of gas phase is pretty high, indicating the cavity composed of the ramp wall and the backward step benefits the combustion of gas phase. The total pressure recovery is a little bit low but still demonstrates that it is possible for the solid-fuel scramjet to operate at a high altitude of low ambient pressure.

5. Conclusion

The solver, namely rhoGasSolidFoam, has been developed on the OpenFOAM platform. Validations show that it is applicable to solving supersonic gas-solid two-phase flows as well as solid-fuel scramjets. A certain configuration of solid-fuel scramjet is presented. Numerical results show that it operates well. The combustion efficiencies of gas and solid phase are 95.3% and 9.6%, respectively, while the total combustion efficiency is 66.6%. The total pressure recovery is 33.4%. The low combustion efficiency of carbon particles results in the not very high total combustion efficiency.

Acknowledgement

This study is supported by the China Scholarship Council.

Reference

[1] Z. Lv, Z.X. Xia, B. Liu, Y.C. Liu, Experimental and Numerical Investigation of a Solid-Fuel Rocket Scramjet Combustor, Journal of Propulsion and Power, 32 (2016) 273-278.

[2] X. Zhao, Z.X. Xia, B. Liu, Z. Lv, L.K. Ma, Numerical study on solid-fuel scramjet combustor with fuel-rich hot gas, Aerosp Sci Technol, 77 (2018) 25-33.

[3] M.A. Witt, Investigation into the Feasibility of Using Solid Fuel Ramjets for High Supersonic/Low Hypersonic Tactical Missiles, in: Naval Postgraduate School Monterey CA, Naval Postgraduate School Monterey CA, 1989, pp. 62.

[4] W.J. Angus, An investigation into the performance characteristics of a solid fuel scramjet propulsion device, in: Naval Postgraduate School Monterey CA, 1991.

[5] A. Ben-Yakar, B. Natan, A. Gany, Investigation of a solid fuel scramjet combustor, Journal of Propulsion and Power, 14 (1998) 447-455.

[6] R. Ben-Arosh, B. Natan, E. Spiegler, A. Gany, Fuel-air mixing in solid fuel scramjet combustors, Int J Turbo Jet Eng, 15 (1998) 223-234.

[7] R. Ben-Arosh, B. Natan, E. Spiegler, A. Gany, Theoretical study of a solid fuel scramjet combustor, Acta Astronautica, 45 (1999) 155-166.
[8] I. Feldman, A. Gany, Parametric Investigation of Supersonic Combustion of Solid Fuels, 5 (2002) 366-374.
[9] S. Saraf, A. Gany, Testing metallized solid fuel scramjet combustor, in: 18th International Symposium on Air Breathing Engines, 2007, pp. 1176-1187.
[10] A. Gany, Accomplishments and challenges in solid fuel ramjets and scramjets, 8 (2009) 421-446.
[11] D. Simone, C. Bruno, Preliminary Investigation on Lithium Hydride as Fuel for Solid-Fueled Scramjet Engines, Journal of Propulsion and Power, 25 (2009) 875-884.
[12] X.Y. Pei, Z.W. Wu, Z.J. Wei, J.Y. Liu, Numerical Investigation on Internal Regressing Shapes of Solid-Fuel Scramjet Combustor, Journal of Propulsion and Power, 29 (2013) 1041-1051.
[13] X.Y. Pei, L.Y. Hou, Numerical investigation on cavity structure of solid-fuel scramjet combustor, Acta Astronautica, 105 (2014) 463-475.
[14] L.H. Wang, S.P. Li, H.W. Chi, B. Li, Z.J. Wei, N.F. Wang, Quasi-One-Dimensional Numerical Method for Solid Fuel Scramjet Combustor Analysis and Design, J Aerospace Eng, 28 (2015).
[15] L.H. Wang, Z.W. Wu, H.W. Chi, C.X. Liu, H. Tao, Q.Y. Wang, Numerical and Experimental Study on the Solid-Fuel Scramjet Combustor, Journal of Propulsion and Power, 31 (2015) 685-693.
[16] H.W. Chi, Z.J. Wei, L.H. Wang, B. Li, Z.W. Wu, Numerical Investigation of Self-Ignition Characteristics of Solid-Fuel Scramjet Combustor, Journal of Propulsion and Power, 31 (2015) 1019-1032.
[17] M. Hu, Z.J. Wei, S.Q. Ding, N.F. Wang, Numerical investigation of a combined solid fuel scramjet combustor, Acta Astronautica, 148 (2018) 210-219.
[18] Y. Liu, Y.G. Gao, L. Shi, Z.X. Chai, X.J. Yu, Preliminary experimental study on solid rocket fuel gas scramjet, Acta Astronautica, 153 (2018) 146-153.
[19] Z. Lv, Z.X. Xia, B. Liu, L.Y. Huang, Preliminary experimental study on solid-fuel rocket scramjet combustor, J Zhejiang Univ-Sc A, 18 (2017) 106-112.
[20] D. Christ, The Effect of Char Kinetics on the Combustion of Pulverized Coal under Oxyfuel Conditions, in: Faculty of Mechanical Engineering, RWTH Aachen University, German, 2013.
[21] S. Kim, B. Natan, Inlet Geometry and Equivalence Ratio Effects on Combustion in a Ducted Rocket, Journal of Propulsion and Power, 31 (2015) 619-631.
[22] B.B. Chen, Z.X. Xia, L.Y. Huang, J.X. Hu, Ignition and combustion model of a single boron particle, Fuel Process Technol, 165 (2017) 34-43.
[23] B. Kalpakli, E.B. Acar, A. Ulas, Improved combustion model of boron particles for ducted rocket combustion chambers, Combustion and Flame, 179 (2017) 267-279.
[24] S. Wang, K. Luo, C.S. Hu, L.Y. Sun, J.R. Fan, Impact of operating parameters on biomass gasification in a fluidized bed reactor: An Eulerian-Lagrangian approach, Powder Technol, 333 (2018) 304-316.
[25] G.M. Faeth, Evaporation and combustion of sprays, Progress in Energy and Combustion Science, 9 (1983) 1-76.
[26] C.T. Cloney, R.C. Ripley, M.J. Pegg, P.R. Amyotte, Laminar burning velocity and structure of coal dust flames using a unity Lewis number CFD model, Combustion and Flame, 190 (2018) 87-102.
[27] D. Toporov, P. Bocian, P. Heil, A. Kellermann, H. Stadler, S. Tschunko, M. Förster, R. Kneer, Detailed investigation of a pulverized fuel swirl flame in CO2/O2 atmosphere, Combustion and Flame, 155 (2008) 605-618.

[28] X.K. Ku, T. Li, T. Lovas, CFD-DEM simulation of biomass gasification with steam in a fluidized bed reactor, Chem Eng Sci, 122 (2015) 270-283.
[29] Z.M. Nikolaou, J.-Y. Chen, N. Swaminathan, A 5-step reduced mechanism for combustion of CO/H2/H2O/CH4/CO2 mixtures with low hydrogen/methane and high H2O content, Combustion and Flame, 160 (2013) 56-75.
[30] M.P. Burke, M. Chaos, Y. Ju, F.L. Dryer, S.J. Klippenstein, Comprehensive H2/O2 kinetic model for high-pressure combustion, International Journal of Chemical Kinetics, 44 (2012) 444-474.
[31] OpenFOAM- the open source CFD tool box- user guide (Version 1806), in, OpenCFD Ltd, https://www.openfoam.com.
[32] F. Alff, U. Brummund, W. Clauss, M. Oschwald, J. Sender, W. Waidmann, Experimental Investigation of the Combustion Process in a Supersonic Combustion Ramjet (SCRAMJET) Combustion Chamber, 1994.
[33] W. Waidmann, F. Alff, M. Bohm, U. Brummund, W. Clauss, M. Oschwald, Supersonic combustion of hydrogen air in a scramjet combustion chamber, Space Technol, 15 (1995) 421-429.
[34] A.S. Potturi, J.R. Edwards, Hybrid Large-Eddy/Reynolds-Averaged Navier–Stokes Simulations of Flow Through a Model Scramjet, AIAA Journal, 52 (2014) 1417-1429.
[35] F. Genin, S. Menon, Simulation of Turbulent Mixing Behind a Strut Injector in Supersonic Flow, Aiaa Journal, 48 (2010) 526-539.